Numerical Modeling of Single Helical Pile Behavior under Compressive Loading in Sand

Lakhdar Salhi

Laboratoire des matériaux et molécules en milieu amazonien,
EcoFoG-Université des Antilles-Guyane,
97351 Cayenne- French Guiana.
e-mail: lsalhi@etu.univ-ag.fr

Ouahcene Nait-Rabah

Laboratoire des matériaux et molécules en milieu amazonien,
EcoFoG-Université des Antilles-Guyane,
97351 Cayenne- French Guiana.
e-mail: ouahcene.nait-rabah@guyane.univ-ag.fr

Christian Deyrat

Guyafor, 97355 Macouria, French Guiana.
e-mail: safor.guyane@wanadoo.fr

Christophe Roos

Laboratoire des matériaux et molécules en milieu amazonien,
EcoFoG-Université des Antilles-Guyane,
97351 Cayenne- French Guiana.
e-mail: christophe.roos@guyane.univ-ag.fr

ABSTRACT

The present research deals with helical piles behavior in cohesionless soil through finite element modeling. An approach of modeling of the screw-pile geometry has been proposed through the Finite Element Analysis (FEA) computer program Plaxis. The numerical results are compared with measurements from large scale test and the bearing capacity has been estimated using both cylindrical and individual bearing model. Moreover, different failure criterions have been applied to estimate the ultimate capacity. The effect of spacing ratio (S/D_h) on the screw-pile behavior has been further studied. It has found that results from the model fit the field results. Through the study of the load transfer mechanism, the transition from cylindrical shear to individual plate behavior occurs at a value of spacing ratio (1.5 to 2).

KEYWORDS: helical pile; finite element method; failure mechanisms, sand.

INTRODUCTION

Helical piles are deep or shallow foundation elements used to provide stability against compressive, tensile and lateral loads. Helical pile behavior in soils has interested a great deal of authors. Several theoretical methods of screw-pile calculation have been developed; these methods are based on the failure models: (1) cylindrical shear model, (2) individual bearing model especially studied by Amy and al. (2009), Zhang et al. (1999) and Andina et al. (2010).

In cohesionless soil, Narasimha (1993) and Zhang et al (1999) showed that, the failure is cylindrical if the ratio of spacing (S) to the average helix diameter (D_h) is lesser than 2. Other studies have shown, each helix develops resistance, if the spacing ratio ($S / D_h \geq 3$) (Donal and Clayton (2005), Canadian and European Offices (2011)). However, there is very little evidence to confirm this assumption (Lutenegger (2011)). Moreover, each helix can behave independently of the others, the pile could be considered as deep foundation.

In order to understand the failure mechanism developed between the anchor and the surrounding soil, several investigations in laboratory have been conducted (Bella (1961), Sutherland et al. (1965), Down and Chieurzzi (1966), Meyerhof and Adams (1968), Clemence and Veesaret (1977), Hoy and Clemence (1989), Narasimha and Rao (1993) and large scale tests studies of helical piles in different soil have been also realized (Saker (2011)). However, few numerical studies available (Ben et al. (2008), Andina and Leonids (2010)).

The finite element analysis is widely used in design of foundation in accordance with the progress of coordinator and more advanced Finite Element software.

The main objectives of this research are:

(a) Comparatives study between the failure criterion applied to load test of helical piles,
(b) To provide a modeling approach of helical piles,
(c) To define the failure mechanism and load transfer behavior for helical piles in sandy soils,
(d) To study the spacing ratio on both load transfer and failure mechanisms.

HELICAL PILE DESIGN

Generally, helical piles design is based on the failure mechanisms (cylindrical shear model or individual bearing model) and on the failure criterion cited below.

Helical Piles Capacity in Compression

For cohesionless soil, the ultimate compression capacity of the helical pile using a cylindrical shearing method (where H/D >=5) as proposed by Mitsch and Clemence (1985) and as referenced in (Helical Pile Engineering Handbook (2010)) is:

$$Q_c = Q_{helix} + Q_{hebottom} + Q_{shaft} \tag{01}$$

$$Q_c = \gamma'.H.A_H.N_q + \frac{1}{2}.\pi.D_a.\gamma'.(H_3^2 - H_1^2).K_s.\tan\varphi + \frac{1}{2}.P_s.H_{eff}^2.\gamma'.K_s.\tan\varphi \tag{02}$$

Where:

Qc - Ultimate compression capacity (kN)
γ_{soil}' - Effective unit weight of soil (kN/m^3)
K_s - Coefficient of lateral earth pressure in compression loading (dimensionless)
φ - Soil angle of internal friction (degree)
A_H - Net area of the bottom helix ($\pi.(D_h^2 - d^2)/4$) (m^2)
Nq - Dimensionless bearing capacity factor
D_a - Average helix diameter (m)
H - The embedment depth of pile (m)
D_1 - Diameter of top helix (m)
H_{eff} - Effective shaft length (m)
H_1 - Depth to top helix (m)
H_3 - Depth to bottom helix (m)
P_s - The perimeter of the helical pile shaft (m)

After design procedure proposed by Adams and Khym (1971), for cohesionless soil, the bearing capacity is given by the following expression:

$$Q_c = \sum Q_h + Q_f \quad (03)$$

$$Q_c = \gamma'.H_1.A_H.N_q + \gamma'.H_3.N_q + \frac{1}{2}.\pi.D_a.\gamma'.(H_3^2 - H_1^2).K_s.\tan\varphi + \frac{1}{2}.P_s.H_{eff}^2.\gamma'.K_s.\tan\varphi \quad (04)$$

Failure Criterion Applied To Load Test of Helical Piles

In many situations the design of foundations is controlled by the allowable structural displacements at foundation level. Therefore, there is a large number of failure criteria used to interpret the axial compressive capacities of helical piles from load test results as described by (Morgan et al (2008), Sakr (2010, 2011), Chance (2006), Ben et al (2008)). The following table summarizes the failure criteria applied on the load test of helical piles.

Table 1: Failure criterions for helical piles.

Brinch Hansen 90% Criterion (Brinch Hansen, 1963),
L1-L2 Method
Davisson's criteria (1972) $QL_P/AE + (D_h/120+4)$ (mm)
Diameter Method QL_P/AE+ (8 à 10 % of pile diameter)
FDOT criteria (FDOT 1999) $QL_P/AE + (D_h/30)$ for $D_h \geq 0.61$m
FHWA criteria (Reese and O'Neill 1988) $5\%D_h$
ISSMFE criteria (ISSMFE 1985) $10\%D_h$
Slope-tangent Method (Butler et Hoy 1977)
Maximum total settlement under a specified load (Chance.2006).
Maximum net settlement after the test load (Chance.2006).

With:

D_h: diameter of the largest helix (mm)
Q: load (kN)
L_p: length of pile (m)
E: modulus of elasticity of pile (MPa)
A: cross section of pile (m^2)

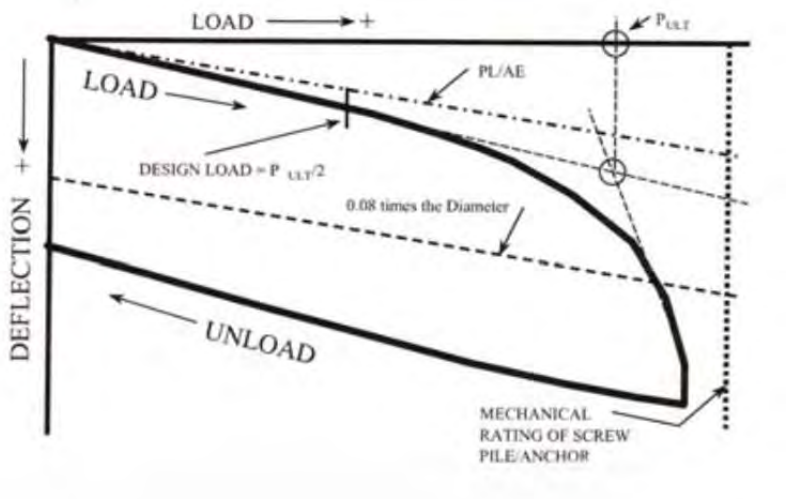

Figure 1: Compression test of helical pile load-displacements curve (Chance, 2006).

According to Chance (2006), failure criterion recommended for helical piles is a net displacement (total displacement less the elastic compression) should not exceed $8\%D_h$ under the half of applied load. A.B. Chance Company uses 8% of the largest helix diameter plus the elastic compression, i.e.$0.08D_h + QL_p/AE$.

Effect of Helical Pile Installation

The installation process of helical piles typically has minimal impact on in-situ soil properties, because of the geometry and the installation method. The center shaft is considered as slender member and causes a relatively small disturbance of the surrounding soil. It can be assumed that all of the helices follow the same path as the lead helix as they are screwed into the ground. In fact, the lead helix cuts a path through the soil and each of the following helices is advanced through the same path, leaving the majority of the soil relatively undisturbed. According to Andrew et al (2011) and Santos et al (2013), the installation process may also cause some unit weight change in the surrounding soil. The effect of this change is minimal in cohesive soils, and is probably most notable in loose to medium dense sands where the void ratio is most readily reduced. However, for both single-helix and multi-helix anchors, the installation may have some influence on the soil. The degree of disturbance is unknown (Lutenegger (2011)).

HELICAL PILE MODELING

In the present study, a modeling of helical pile in sandy soil under compressive load was conducted. The static axial loading test have been modeled and analyzed using the FE software Plaxis 2D as described in Figure 2.

A linear elastic–perfectly plastic Mohr–Coulomb model (MCM) was chosen to describe the soil. Drained behaviour was assigned for all layers, due to the high permeability of sandy material. Whereas, linear elastic and Coulomb criterion were especially used for pile and interface.

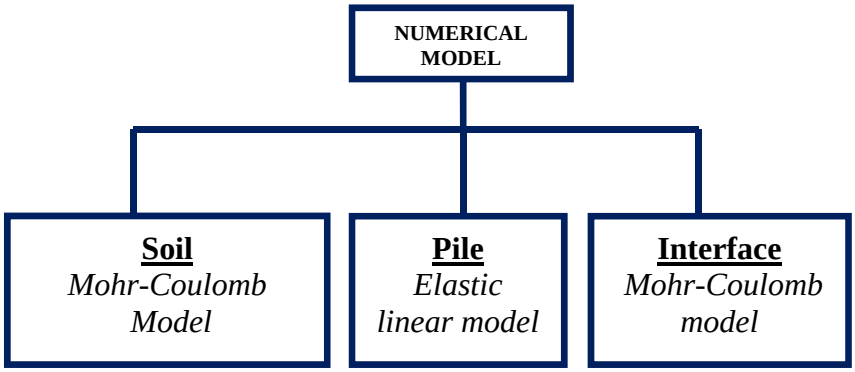

Figure 2: Numerical model.

Interface Behavior

Through this study, interface elements were incorporated along the pile to simulate the soil-pile interaction. An elastic plastic model based on the Coulomb criterion was used to describe the interface behavior. The strength proprieties of interface were linked to the strength proprieties of the soils layers. Each data set had an associated strength reduction factor, R_{inter} for interfaces in plaxis as follows:

For the elastic behavior, the shear stress is defined by:

$$\tau \leq -\sigma_n \tan\varphi_i + C_i \tag{05}$$

For the plastic behavior, the shear stress is defined by:

$$|\tau| = -\sigma_n \tan\varphi_i + C_i \tag{06}$$

The reduction factor also is defined by:

$$C_i = R_{\text{int}\,er}.C_{soil} \tag{07}$$

$$\tan\varphi_i = R_{\text{int}\,er}.\tan\varphi_{soil} \leq \tan\varphi_{soil} \tag{08}$$

$$\text{If } R_{\text{int}\,er} \lhd 1,\ \psi_i = 0^\circ \text{ , otherwise } \psi_i = \psi_{soil} \tag{09}$$

with:

C_i	Cohesion of the interface	(kN/m^2)
C_{soil}	Cohesion of soil	(kN/m^2)
σ_n	Normal stress at the interface	(kN/m^2)
τ	Shear stress	(kN/m^2)
φ_i	Friction angle of the interface	(°)
φ_{soil}	Friction angle of the soil	(°)
ψ_i	Dilatancy angle of the interface	(°)
ψ_{soil}	Dilatancy angle of the soil	(°)
R_{inter}	Interface factor	--

State of Stress

In order to understand the failure mechanism of helical piles under compressive loading, it is most convenient to assess the state of stress in the soil in terms of the relative shear stress. The relative shear stress is defined as:

$$\tau_{rel} = \frac{\tau_{mob}}{\tau_{\max}} \tag{10}$$

where: τ_{mob} is the maximum value of shear stress (i.e., the radius of the Mohr stress circle). The parameter $\tau_{\max}$ is the maximum value of shear stress when the Mohr's circle expanded to touch the coulomb failure envelope, keeping the intermediate principal stress constant. Thus a relative shear stress value of $\tau_{rel} = 1$ is indicative of soil failure. The maximum shear stress is defined as:

$$\tau_{\max} = -\frac{\sigma_1^{'} + \sigma_3^{'}}{2}\sin\varphi + C\cos\varphi \tag{11}$$

Geometry Modeling and Materials Parameters

An axisymmetric condition was assumed to model this geometry in two-dimensional space. This condition can be used for circular structures with an almost uniform cross section with load distribution around the central axis. In axisymmetric condition, the x-coordinate represents the radius, and the y-coordinate denotes the axial line of symmetry. In this study, we proposed to model the pipe helical pile with elements no-porous (permeability is equal to zero) available in plaxis. The helix plates were modeled as circular disks. Interface elements were incorporated along the pile to simulate the soil-pile interaction.

Helical piles are installed with applied torque at the pile head. Table 2 provides a resume of geometrical parameters of the piles Figure 3), the maximum torque of installation and depth of embedment. Table 3 provides the parameters of pile materiel.

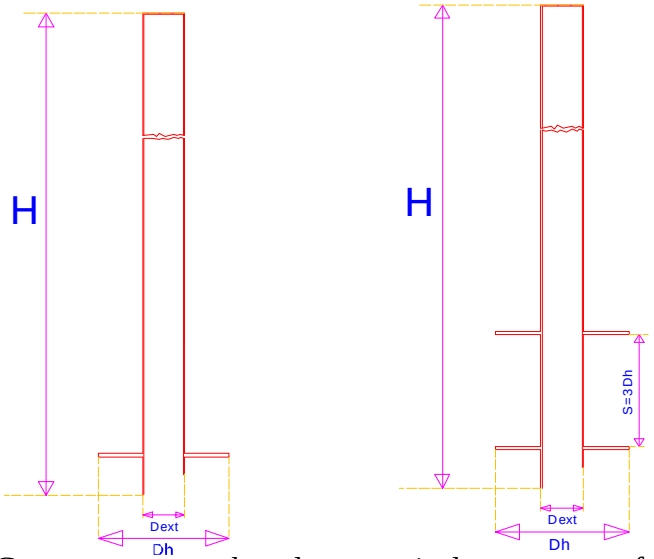

Figure 3: Geometry approach and geometrical parameters of tested piles.

Table 2: Piles configurations and installation

Pile type	*shaft*		*Helix*			*S*	*H*	*Installation Torque*
	diameter d (mm)	thickness e (mm)	Diameter D_h (mm)	thickness e* (mm)	N^O helix	spacing (m)	Depth (m)	T (kN.m)
P1	324	9.5	762	25.4	2	$3*D_h$	9	211.5
P2	324	9.5	762	25.4	1	-	9.5	211.5
P3	406	9.5	914	25.4	1	-	6.1	338.3
P4	508	9.5	1016	25.4	1	-	5.75	338.3

Table 3: Piles parameters

parameters			***Disks***	***Shaft***
	model		linear Elastic	linear Elastic,
	type		non-porous	non-porous
γ_p	Pile unit weight	kN/m^3	78	78
K_x,k_y,k_z	Permeability	m/day	NA	NA
υ	Poisson's ratio		0.3	0.3
E	Modulus of elasticity of pile	kN/m^2	21.10^7	21.10^7

Young's modulus from triaxial experiments results (reference pressure P_{ref} = 100KPa) is given by the relations summarized in Table 4 (Schanz and Vermeer (1998)). These piles were installed in cohesionless soil (sandy soil). The phreatic level is at -3.6m below ground surface. The parameters of the layers are given in Table 5.

Table 4: Young's modulus from Triaxial experiments results

Sand	*Vermeer et schanz*
Loos or silt	$\frac{E_{50}}{p_{ref}} = 150.\sqrt{\frac{\sigma'_y}{p_{ref}}}$
Dense	$\frac{E_{50}}{p_{ref}} = 500.\sqrt{\frac{\sigma'_y}{p_{ref}}}$

σ'_y is the effective vertical stress at the mid depth of each layer. For numerical stability, cohesion is taken equal to 1. In addition, the dilatancy angle is evaluated by the recommended formula ($\psi = \varphi' - 30$) such as:

$$\psi = \varphi' - 30 \quad \text{for} \quad \varphi' \succ 30$$

$$\psi = 0 \quad \text{for} \quad \varphi' \prec 30$$

Table 5: Materials proprieties of the sand layers

proprieties			soil	
			Layer 1	Layer 2
	model		MCM	MCM
	drainage state		drained	drained
γ_{unsta}	Soil unit weight above phreatic level	kN/m^3	18	20
γ_{sat}	Soil unit weight below phreatic level	kN/m^3	20	21
ν’	Poisson’s ratio	-	0.33	0.33
C’	cohesion	kN/m^2	1	1
φ'	Friction angle	degree	35	40
Ψ’	Dilatancy angle	degree	5	10
Cu	Untrained shear stress	kN/m^2	-	-
E_{50}^{ref}	Young’s modulus	MPa	48	77

Initial Conditions

The initial conditions are geostatistical stress representing the weight of soil layers. This state is defined by both vertical and horizontal effective stresses.

$$\sigma'_{h,0} = K_0 . \sigma'_{v,0} \tag{12}$$

In Plaxis, for Mohr-Coulomb model the value of k_0 is defined by Jacky formula ($k_0 = 1 - \sin\varphi'$).Hydrostatic pressures are generated in the whole geometry according to this level. The unit weight of water is set to default value 10kN.m^{-3}.

Boundary Conditions and Model Limits

According to Mestat and Prat (1997, 2010), to minimize boundary effects on pile response, it is important to fix the horizontals and verticals boundaries of the model as follow:

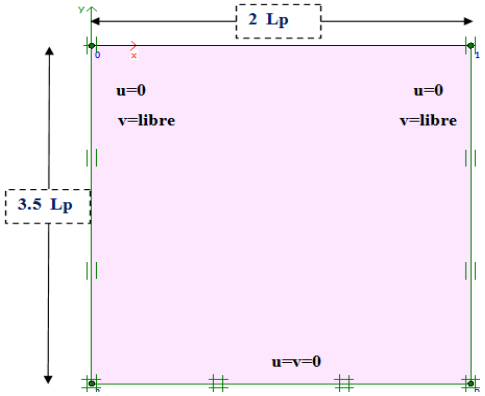

Figure 4: Boundary conditions (where L_p is the pile length (m))

As shown in figure 4, the boundary conditions are:

(a) Vertical model boundaries with their normal in x-direction are fixed in x-direction ($u_x = 0$) and free in y-direction,

(b) The model bottom boundary is fixed in all directions ($u_x = u_y = 0$).

(c) The ground surface of the model is free in all directions.

Mesh Generation

Plaxis allows for automatic generation of unstructured finite element meshes. During the generation of mesh, 15-node triangular elements were selected in order to provide greater accuracy in the determination of displacements. In the present study, medium with local mesh refinement are used. The mesh is refined around the pile (Figure 5).

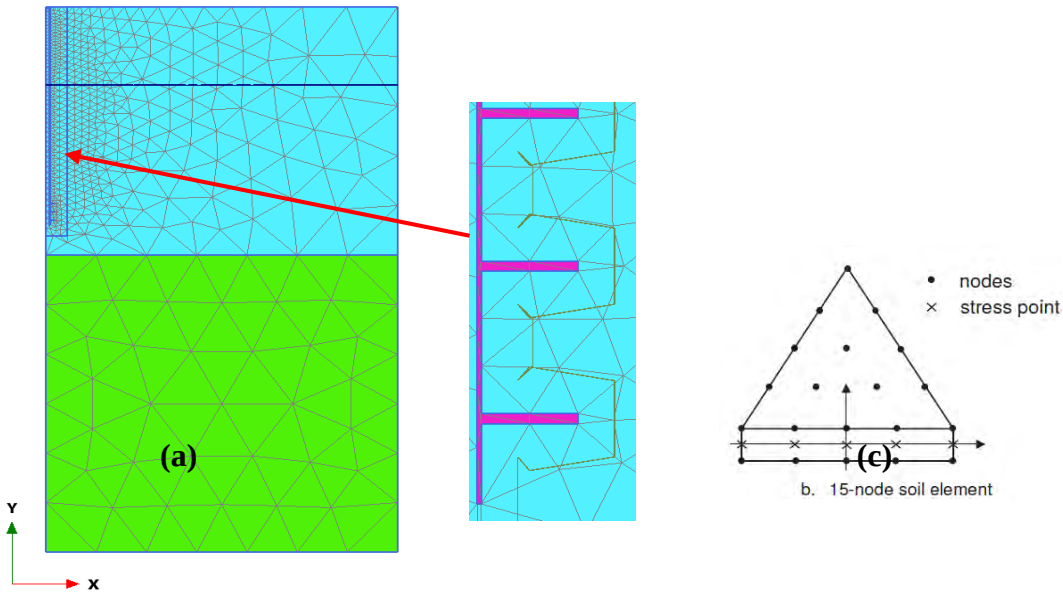

Figure 5: (a) Full mesh of the model, (b) view of the pile in soil, (c) interface-soil connection (soil element: 15 nodes, interface element: 5 nodes)

Analysis Phases

We have reproduced the static loading test of a single pile on PLAXIS (2011). Through this modeling, we can define the evolution of resistances and displacements for each load increment. Plaxis analyses were run in phases as follow:

Initial phase (0): initial conditions

The initial conditions taken in to account are: the initial groundwater conditions, the initial geometry configuration and the initial effective state. The calculation type is k_0 procedure to generate initial effective stresses. In this phase, pile cluster should be changed by soil as shown in Figure 6.

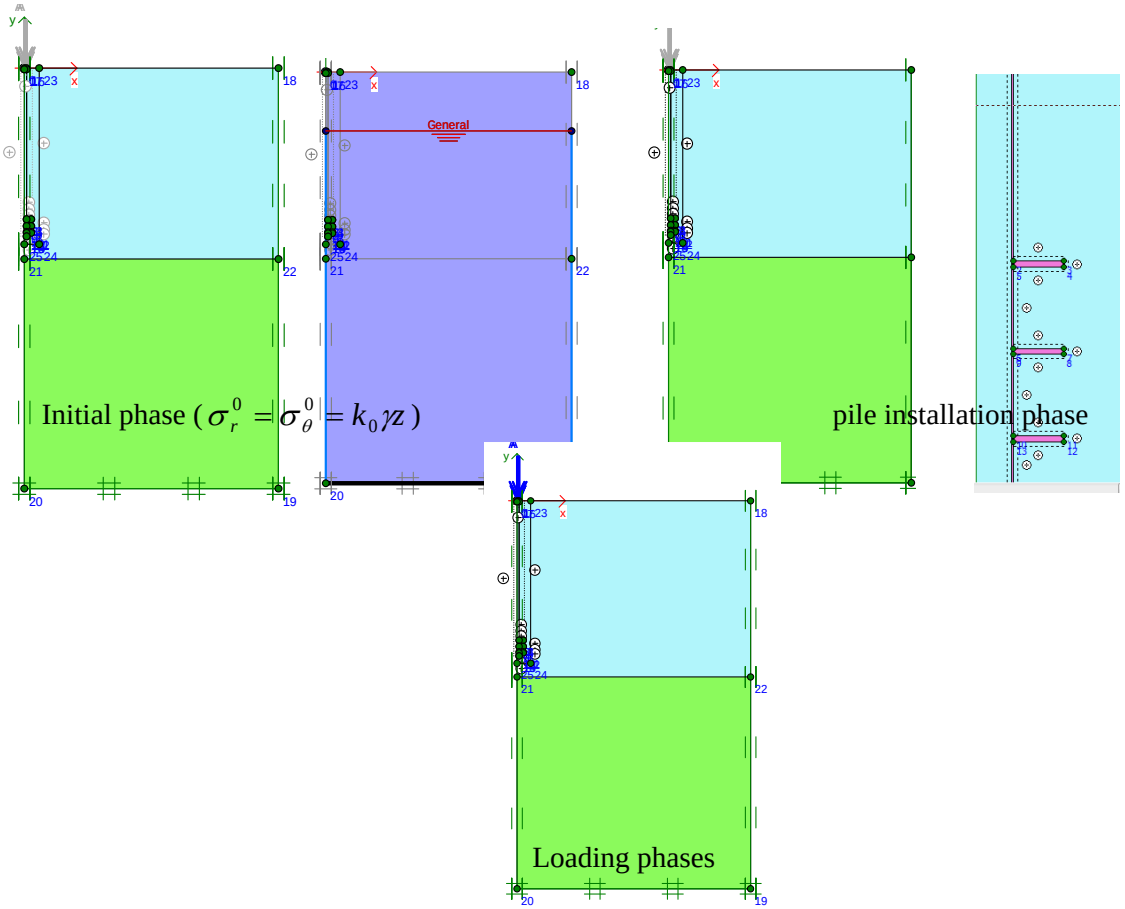

Figure 6: Calculation phases

Phase (1): Pile installation

In order to simulate the settlement of the pile in analysis, a plastic calculation is required. Then the material of the pile cluster is replaced by pile material and, interfaces between soil and pile are activated. Here, we assume that the helical pile is completely full of soil at the end of the installation.

Phase (2): Pile loading

At this stage we assume the pile installation process to be modeled, and start the pile load test. First a unit distributed load is activated at the pile head. Subsequently this load is increased until the automatic load-increment routine in the FE program. However, the pile installation process is simulated directly after the initial stress generation. Then, the load is manually incremented (using incremental multipliers) (0-2227kN).

RESULTS AND DISCUSSION

Load-settlements curves and failure criterion

The load-movement curves for both numerical and experimental curves are shown in the Figure 7. Table 6 provides the ultimate capacity of helical piles calculated with different failure criterions.

Table 6: Ultimate capacity calculated with different failure criterions

piles	*Capacity (KN)*	*Davisson method*	*FDOT method*	*FHWA criterion*	Diameter method $QL_p/EA+8\%d$
P1	Experimental	1100	1810	2030	1859
	Numerical	1206	1747	1910	1765
P2	Experimental	1088	1801	1944	1849
	Numerical	1158	1647	1750	1700
P3	Experimental	1456	2288	2450	2311
	Numerical	1201	1992	2288	2033
P4	Experimental	1178	1948	2188	2094
	Numerical	1062	1751	2048	1920

The results obtained from numerical simulation were confronted with experimental results from a large scale test. The load-movement curves obtained from compression tests for both numerical and experimental test are presented in the Figure 7 (*continues on the next page*).

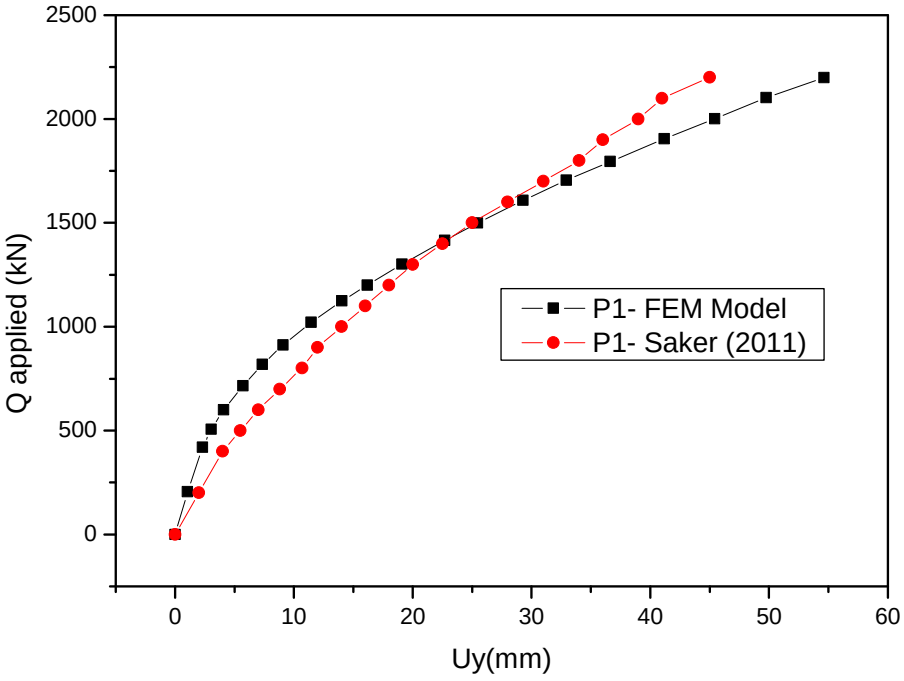

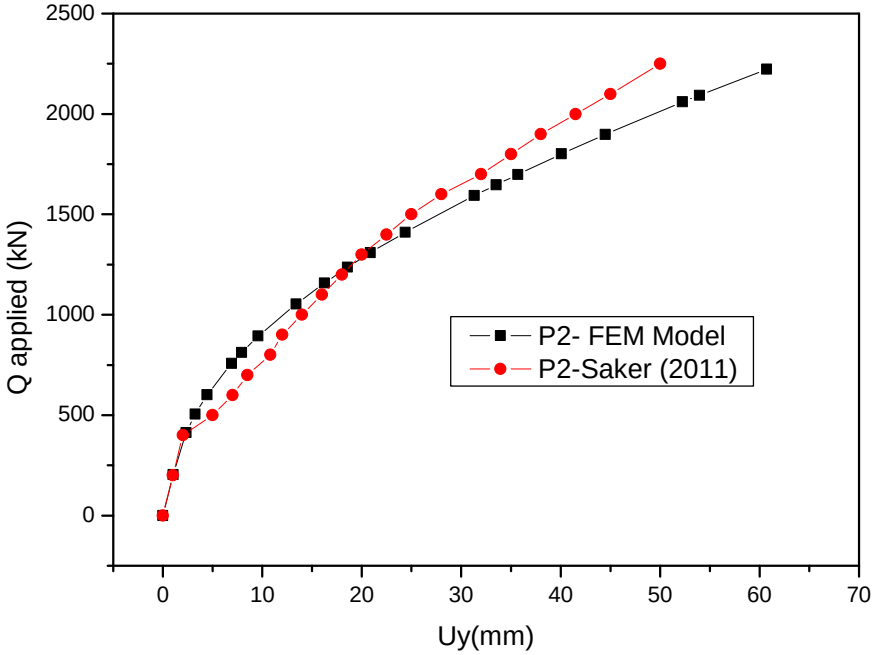

Figure 7: Failure criterions applied for load test ((a) 2 helix (D_h=762mm, d=324mm, S=3D_h, H=9m), (b) 1 helix (D_h=762mm, d=324mm, H=9.5).

According to the results in the Table 4 above, Davisson failure criterion is the most pessimistic that is widely used for estimating the axial capacities of piles (Chance (2003), Saker (2011)). The average relative error compared to the most optimistic method (FHWA) is 42%. We also noted, for λ (D_h/d) =2.4, FDOT and diameter criteria (QL_p / EA +8% d) give the same results. The relative error between the two methods increases with decreasing of λ, it ranges from 1 to 8%. The average relative error between FDOT and FHWA methods is about 9%. FHWA criterion (5% D_h) gives the larger capacity compared to other methods. As shown in load-displacement curves, we found consistency between numerical and experimental results.

Ultimate Capacity by Different Methods

The two theoretical methods cited above have been applied to estimate the ultimate compressive capacity for all tested piles. In the present study, the ultimate capacities of helical piles were defined as the load level that produce a displacement equal to 5% of the diameter of the largest helix. The comparison of the predicted results using both cylindrical shear and individual bearing methods are presented in the Table 5.

Table 7: Ultimate compressive capacity by different methods

Sand			**capacity in compression (kN)**			
Method type	Failure model	Methods	Q (P1) (kN)	Q (P2) (kN)	Q (P3) (kN)	Q (P4) (kN)
direct Methods	cylindrical shear model (kN)	Mitsh and Clemence method (1985)	1770	1772	1750	2000
	Individual bearing method (kN)	Individual Plate Capacity (IPC) Method	2984	1772	1750	2000
	Experimental capacity (kN)	Tests in-site (5%)	2030	1944	2450	2188
Plaxis 2d (2011)		Plaxis simulations (5%)	1910	1770	2288	2048

For the compression test, a cylindrical shear model from Mitsh and clemence method (1985) provides a better prediction for Helical pile with $S/D_h=3$. The average relative error with experimental and numerical capacity is 12%. However, the average relative error is 30% for individual bearing model. The average relative error between experimental and numerical capacities varies from 5 to 8%.

Spacing Ratio Effect on the Helical Pile Behavior in Sand

Currently, in sand, suggestions have been made that the transition from cylindrical shear to individual plate behavior occurs at relative spacing equal to 3. However there are essentially no published data to confirm this assumption (Lutenegger (2011)). The experimental results of Zhang (1999) shown, for compression tests of helical piles in cohesionless soil, the cylindrical surface failure provides a better prediction for spacing ratio ($S/D_h \leq 2$). In order to study the effect of S/D_h on the helical pile behavior under axial compressive loading, we proposed the piles configurations as shown in the Table 8.

Table 8: Piles configurations

Pile type	*shaft*		*Helix plates*			*S*	H_1	*H*
	diameter Dext (mm)	thickness e (mm)	diameter Dh (mm)	thickness d (mm)	NO helix	spacing (m)	Depth to top helix (m)	Depth (m)
5	324	9.5	762	25.4	3	0.5*Dh	9.013	10
5	324	9.5	762	25.4	3	1.0*Dh	8.250	10
7	324	9.5	762	25.4	3	1.5*Dh	7.489	10
8	324	9.5	762	25.4	3	2.0*Dh	6.727	10
9	324	9.5	762	25.4	3	2.5*Dh	5.965	10
10	324	9.5	762	25.4	3	3.0*Dh	5.203	10
11	324	9.5	762	25.4	3	3.5*Dh	4.441	10

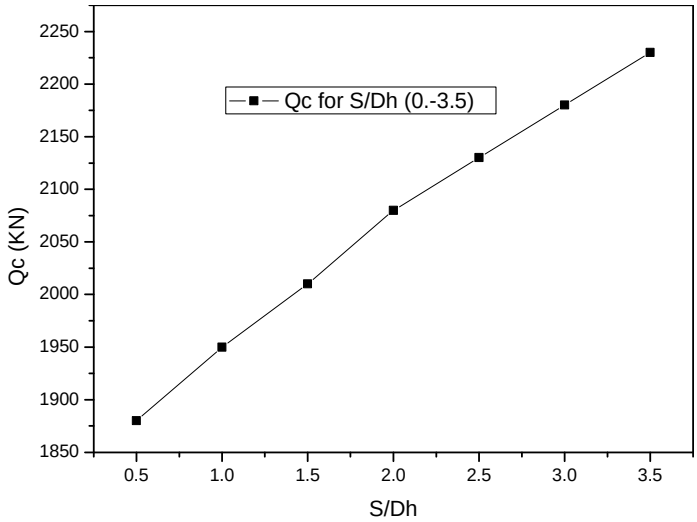

Figure 8: Capacity at compression load for different S/D_h

The behavior of multi-helix helical piles installed in cohesionless soil is dependent upon the spacing ratio. The load-settlement curves (Figure 8 and 9) demonstrated an increase in the compression capacity with the increasing of S/D_h. For a load lower than 500 kN; all piles have the same behavior regardless the spacing ratio. We can explain these phenomena by the load transfer to the helix plates. So, with increasing of spacing ratio, each helix develops resistance, this is confirmed by the load-helix resistances curves shown in the Figures (10).

The Load-bottom helix resistance curves (Figure 10 (a)) show that for loading from 0 to 500 kN, the bottom helix resistance is almost constant for different spacing ratio (S/D_h).

For higher load, the bottom helix resistance increases with load and decreases with increasing of S/D_h. Moreover, we find that the bottom helix resistance is stabilized for $S/D_h > 1.5$. For a load greater than 500kN, both middle and top helix resistances increase with the increase of S/D_h (Figure 10 (b) (c)).

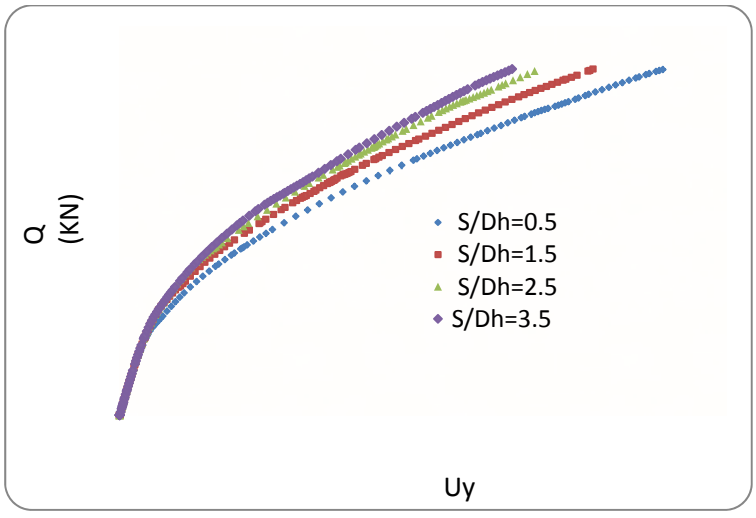

Figure 9: Load-displacement curves for different values of S/D_h

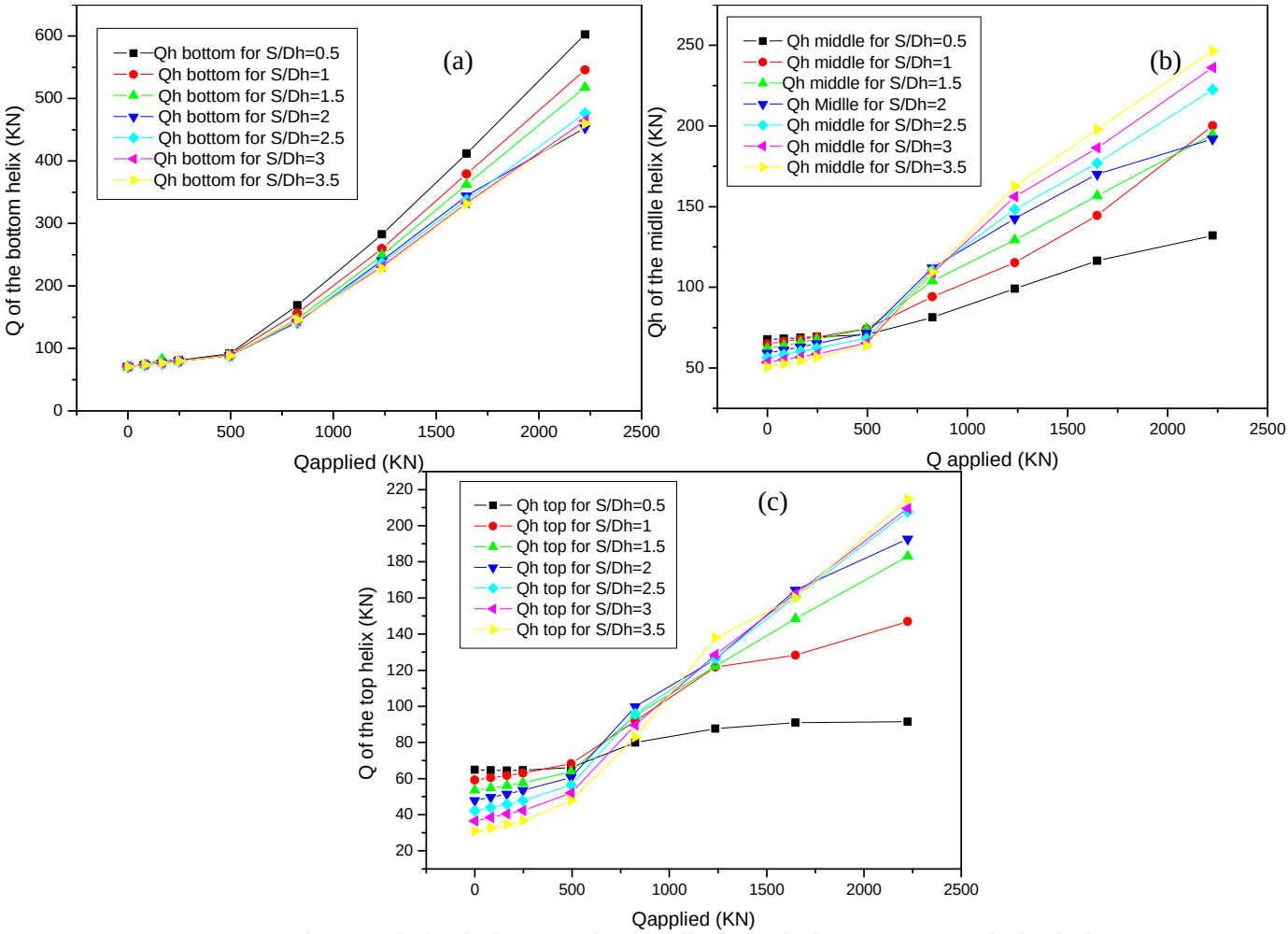

Figure 10: (a) bottom helix behavior, (b) middle helix behavior, (c) top helix behavior for different values of S/Dh

The range 0-500 kN corresponds at the mobilization of skin friction as shown in the lateral friction-displacement curves (Figure 11). The friction along the shaft is calculated using the following expression:

$$Q_{s,n} = \int_0^L \tau(y).2.\pi.R.dy = \sum_1^i \tau(y_i).2.\pi.R.L \qquad (13)$$

Where: dy=L/i; i: number of segments of thickness dy,

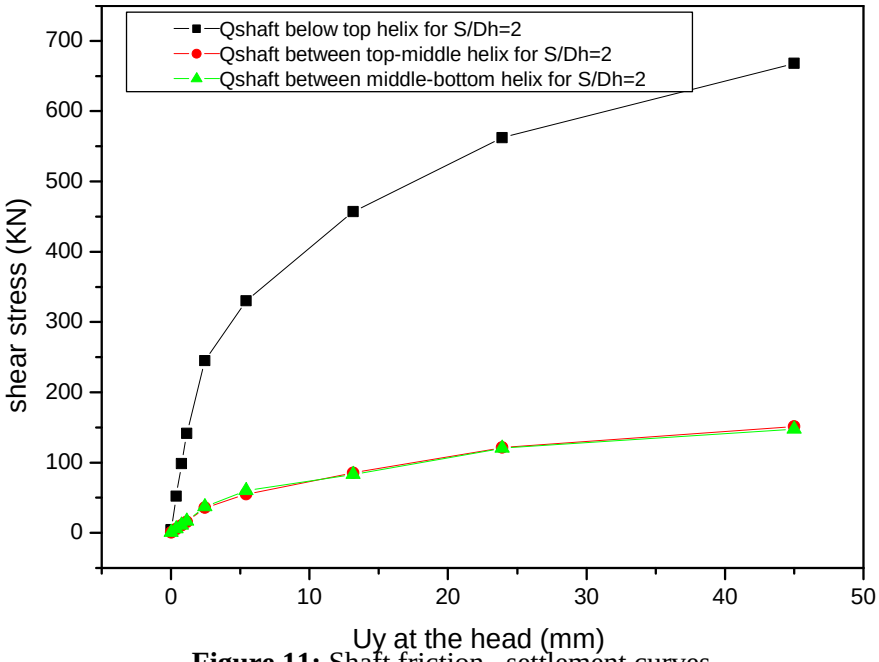

Figure 11: Shaft friction– settlement curves

For the comparison between the response of the three helix depending on both the applied load and spacing ratio S /D_h, the (Figure 12 (a, b, c, d), shows, that the middle and top helix resistances increase when S/D_h increases. These resistances become notable for spacing ratios S/D_h > 1.5. However, the resistance of the bottom helix is the most important.

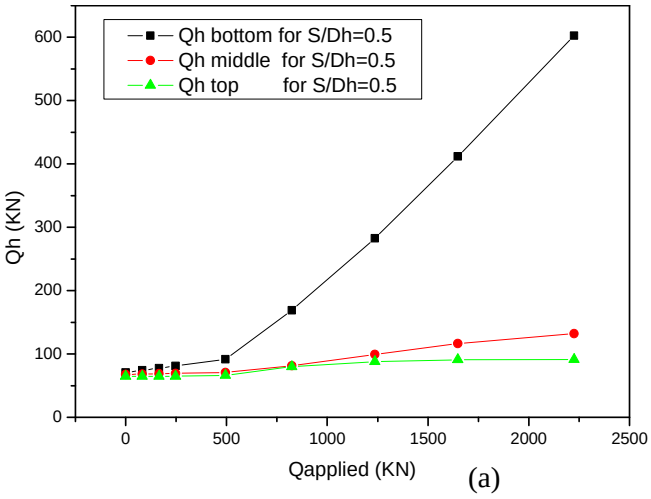

(a)

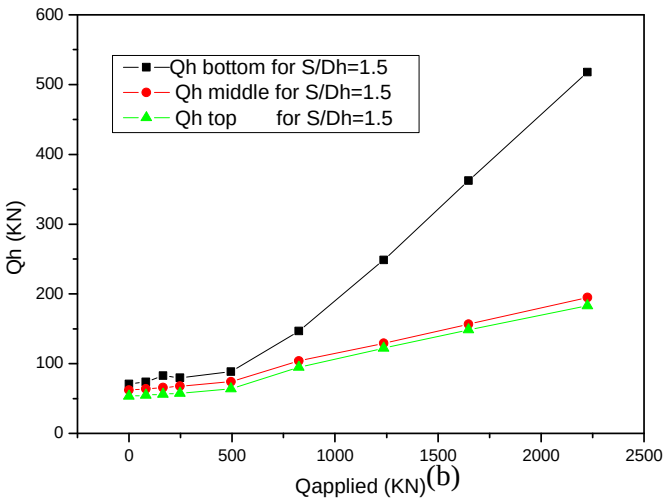

(b)

(*Continues on the next page*)

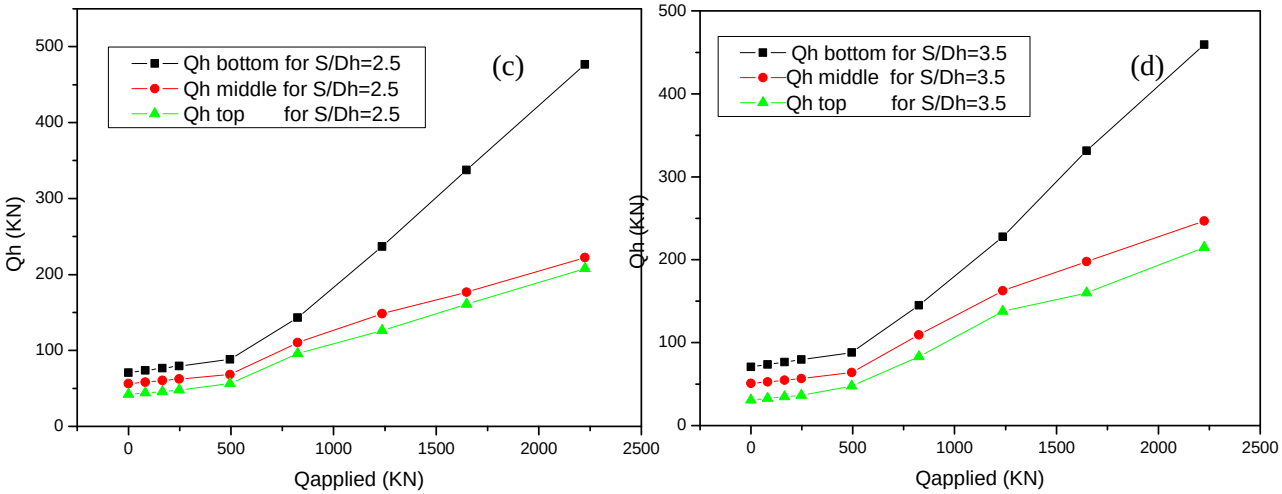

Figure 12: Bottom, middle and top helix behavior for different S/Dh, (a) S/Dh=0.5, (b) S/Dh=1.5, (c) S/Dh=2.5, (d) S/Dh=3.5

Relative Stresses and Displacements Contours

In order to better understand the failure mechanism of helical piles under compressive loading, it is most convenient to analyze the state of stress in the soil in terms of the relative shear stress and displacement of the soil. The Figure 13 displays the behavior of helical piles under compressive loading for different values of S/D_h. This result is shown in terms of relative shear stress and displacement at failure.

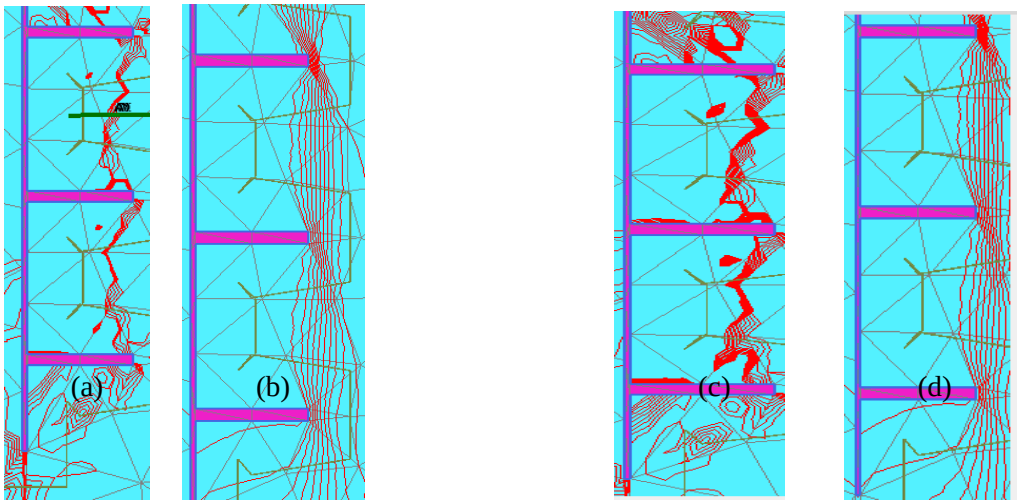

(*Continues on the next page*)

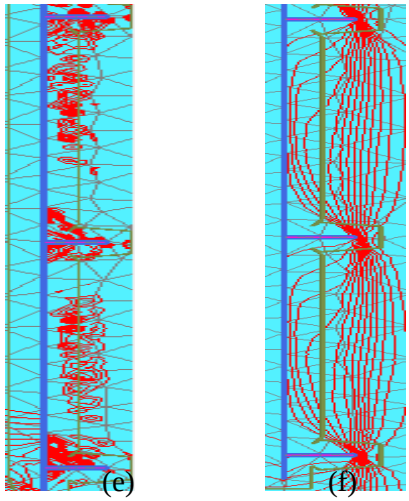

Figure 13: Relative shear stress and soil displacements for (1) : S/D_h=0,5: (a) $\tau_{rel} = 0.9-1$; (b) Uy (12-48mm); for (2) : S/D_h=1,5: (c) $\tau_{rel} = 0.9-1$; (d) Uy (28-46mm); for (3) : S/D_h=2,5; (e) $\tau_{rel} = 0.8-1$; (f) Uy (10-37mm).

The maximum relative shear stress contour is located to the exterior contour and the displacement is maximum at the interior contour. For higher spacing ratio ($S/D_h \geq 1.5$), bearing failure occur under each helix without interference with each other as represented in (Figure 13 ((e) and (f))). This variation of the relative shear stress and displacement with the spacing ratio confirm the results discussed above.

CONCLUSION

Based on the results of the numerical study of helical piles behavior under compressive load, the following conclusions can be drawn:

a) We can recommend the modeling of helical pile in plaxis with non-porous elements for better reproducing the helical piles behavior. The helix plates can be molded by disks.

b) The load distribution results indicated a general cylindrical shearing surface was formed at failure. Therefore, the total resistance consists of three components: shaft resistance, cylindrical shearing resistance and the bearing resistance of the helix plates. We demonstrated that, the bottom helix resistance develop a higher resistance then the others helix regardless the spacing ratio (S/D_h).

c) With the increasing of spacing ratio, we have a load transfer from the bottom helix to the both middle and top helix. There is a significant increase in capacity with the increase of spacing ratio.

d) For this case, we also showed that the both middle and top helix develop resistances at spacing ratio between 1.5 and 2. Therefore, the transition from cylindrical shear to individual plate behavior occurs at relative spacing: 1.5 to 2.

e) For a load lower than the load of skin friction mobilization; all piles have the same behavior regardless the spacing ratio (S/D_h).

ACKNOWLEDGEMENTS

This work was supported by European Union through PROMES framework (European Development Funds, program: No.31567) and the PhD grant by ANRT-Agency (CIFRE No 975/2011).

REFERENCES

1. Amy B. and Cerato, P. E. (2009) "Effects of Long-Term Dynamic Loading and Fluctuating Water Table on Helical Anchor Performance for Small Wind Tower Foundations," Journal of Performance of Constructed Facilities, Vol. 23, No. 4, pp 251-261.
2. Andina, S. and Leonids, P (2010) "Helical pile behaviour and load transfer mechanism in different soils," International conference (Modern building materials structures and techniques), pp 1174-1180.
3. Andrew P. and Adams, P. E. (2011) "Helical Pile Application and Design," PhD engineer, LLC, pp 1-15.
4. Bella, A. (1961) "The resistance to breaking-out of mushroom foundations forpylons," Proceeding of the 5the international conference of soil mechanics and foundation engineering, Paris, France, Vol.1, pp 269-576.
5. Ben L. and Hesham El Naggar M (2008) "Axial testing and numerical modeling of square shaft helical piles under compressive and tensile loading," Canadian Geotechnical Journal, No.45, pp 1142-1155.
6. Chance (2003) "Helical Screw Foundation System Design Manual for New Construction," Copyright Hubbell, Inc., step 5, pp 1-8.
7. Chance (2006) "Design methodology section 5," Hubbell Power Systems, Inc., Vl.0, pp 1-27.
8. Chance (2006) "Load Tests Appendix B," Hubbell Power Systems, Inc.,V1.0, pp B1-B13.
9. Clemence, S.P. and Veesaert, C.J (1977) "Dynamic pullout resistance of anchors in sand," In proceedings of international symposium on soil-structure interaction.Roorkee, India, pp 389-397.
10. Donal J. and Calyton P. E (2005) "Basic helical screw pile design," ECP torque Anchor Brand of helical screw piles, Earth Contact Products, pp 1-28.
11. Downs, D.I. and Chieurzzi, R (1966) "Transmission Tower Foundations," Journal of the Power Division, ASCE, Vol. 92, No.02, pp 91-114.
12. Hoy, R. M. and Clemence, S.P (1989) "Uplift of helical anchors in soil," In proceedings of the 12th international conference of soil mechanics and foundation engineering (ISSMFE), Rio de Janeiro, Brazil. Vol.2, pp 1019-1022.
13. Hoyt, R. M. and Clemence, S. P (1989) "Uplift capacity of helical anchors in soil. International conference on soil mechanics and foundation engineering," Chance, A. B. Bulletin N.02-9001.
14. Howard, A. P (2009) "Helical Piles: Bearing Capacity," John Wiley and Sons, Inc, pp 103-149.

15. Head Office and Canadian Offices (2010) “European Offices. Helical Pile Engineering Handbook,” HPS 7th Edition, pp 20-28.

16. Hamed, N., Khairul, A. K., Amin, G., Ramli, N. and Chuan, H.S (2012) “Performance of Helical Anchors in Sand,” Electronic Journal of Geotechnical Engineering, Vol. 1, Bund. R., pp 2683-2702.

17. Lutenegger, A. J (2011) “Behavior of Multi-Helix Screw Anchors in Sand,” Proceedings of the 14th Pan- American Conference on Soil Mechanics and Geotechnical Engineering.

18. Meyerhof, G. G. and Adams, J. I (1968) “The ultimate uplift capacity of foundations,” Canadian Geotechnical Journal, Vol.4, N0.5, pp 225-244.

19. Morgan W.N. and Timothy C.S (2008) “Shortcomings of the Davisson Offset Limit Applied to Axial Compressive Load Tests on Cast-In-Place Piles,” Deep foundation Journal, pp 568-574.

20. Narasimha R. S. and Prasad, Y (1993) “Estimation of uplift capacity of helical piles in clays,” Journal of Geotechnical Engineering, Vol 119, N0.2, pp 352-357.

21. Philippe, M (1997) “Maillage d’éléments finis pour les ouvrages de géotechnique : conseils et recommandations, ” Bulletin des laboratoires des ponts et chaussées-No.212, pp 39-64.

22. Sakr M (2011) “Installation and performance characteristics of high capacity helical piles in cohesionless soils,” DFI Journal, Vol 5, No.1, pp 39-57.

23. Santos,T. C., Tsuha C. H. C. and Giacheti H. L (2013) “The use of CPT to evaluate the effect of helical pile installation in tropical soils,” Geotechnical and Geophysical Site Characterization 4, Coutinho & Mayne (eds), Taylor & Francis Group, London, pp 1079-1084.

24. Zhang D. (1999) “Predicting Capacity of Helical Screw Piles in Alberta Soils” MSc. thesis, University of Alberta, Edmonton, Alberta, Canada.